

Impact of the Indian Ocean Dipole on Evolution of the Subsequent ENSO: Relative Roles of Dynamic and Thermodynamic Processes

ZHANG YUE,^a W. ZHOU,^a AND TIM LI^{b,c}

^a *Guy Carpenter Asia-Pacific Climate Impact Centre, School of Energy and Environment, City University of Hong Kong, Hong Kong, China*

^b *International Pacific Research Center, University of Hawai'i at Mānoa, Honolulu, Hawaii*

^c *Department of Atmospheric Sciences, University of Hawai'i at Mānoa, Honolulu, Hawaii*

(Manuscript received 26 June 2020, in final form 19 January 2021)

ABSTRACT: The complex interaction between the Indian Ocean dipole (IOD) and El Niño–Southern Oscillation (ENSO) is further investigated in this study, with a focus on the impacts of the IOD on ENSO in the subsequent year [ENSO(+1)]. The interaction between the IOD and the concurrent ENSO [ENSO(0)] can be summarized as follows: ENSO(0) can trigger and enhance the IOD, while the IOD can enhance ENSO(0) and accelerate its demise. Regarding the impacts of IOD(0) on the subsequent ENSO(+1), it is revealed that the IOD can lead to anomalous SST cooling patterns over the equatorial Pacific after the winter following the IOD, indicating the formation of a La Niña–like pattern in the subsequent year. While the SST cooling tendency associated with a positive IOD is attributable primarily to net heat flux (thermodynamic processes) from autumn to the ensuing spring, after the ensuing spring the dominant contribution comes from oceanic processes (dynamic processes) instead. From autumn to the ensuing spring, the downward shortwave flux response contributes the most to SST cooling over the central and eastern Pacific, due to the cloud–radiation–SST feedback. From the ensuing winter to the ensuing summer, changes in latent heat flux (LHF) are important for SST cooling, indicating that the release of LHF from the ocean into the atmosphere increases due to strong evaporation and leads to SST cooling through the wind–evaporation–SST feedback. The wind stress response and thermocline shoaling verify that local Bjerknes feedback is crucial for the initiation of La Niña in the later stage.

KEYWORDS: Air–sea interaction; ENSO; Heat budgets/fluxes; Indian Ocean

1. Introduction

The El Niño–Southern Oscillation (ENSO) cycle is the dominant interannual air–sea coupling mode in the Pacific; it is composed of alternating warm El Niño and cold La Niña events and can exert significant global impacts through interactions between ocean basins and the atmosphere (McPhaden et al. 2006; Wang et al. 2009, 2012). The Indian Ocean dipole (IOD) is also an important interannual variation mode in the Indian Ocean, with abnormal cooling SSTs off Sumatra and anomalous warming SSTs over the western equatorial Indian Ocean (Saji et al. 1999; Webster et al. 1999). It has been extensively revealed that SST variation in the Indian Ocean will induce anomalous atmospheric responses over East Asia (e.g., Leung et al. 2020; Zhang et al. 2019b; Chen et al. 2018b; Wu et al. 2009a; Xie et al. 2009). Previous work has shown that the IOD, as the inherent oscillation mode in the Indian Ocean, is independent of ENSO (Saji and Yamagata 2003; Behera et al. 2006; Luo et al. 2008; Gu et al. 2009; Yuan et al. 2008a), which has significant influence on the Asian climate (Kripalani et al. 2010; Ashok et al. 2004; Cai et al. 2011; Zhang et al. 2019a,b; Yuan et al. 2008b; W. Wang et al. 2014; Wang et al. 2006; Chen et al. 2018a). However, ENSO, as the strongest interannual oscillation in the tropics, is highly likely to have impacts on IOD variability (e.g., Alexander et al. 2002; Ham et al. 2013; Chen et al. 2013; Zhang et al. 2015; Dong and McPhaden 2017).

For example, Gualdi et al. (2003) found that ENSO can create favorable circulation conditions for the development of the IOD over the southwestern Indian Ocean. Behera et al. (2006) used numerical simulation to show that ENSO has a modulation effect on the IOD by influencing its periodicity, intensity, and structure. Yuan et al. (2008c) also identified a modulating impact of ENSO on the structure of the IOD, where the warming pole of the positive IOD tends to be shifted northwestward when it occurs with El Niño. Meanwhile, ENSO can induce easterly anomalies over the eastern Indian Ocean and then trigger the IOD by modulating the convection center and the Walker circulation (Ueda and Matsumoto 2000; Annamalai et al. 2003; Fischer et al. 2005).

On the other hand, the complexity of the interaction between the IOD and ENSO also lies in the ability of the IOD to influence the ENSO cycle. The IOD can influence the co-occurring ENSO cycle by amplifying its strength (e.g., Luo et al. 2010) and by accelerating its phase transition (e.g., Izumo et al. 2016). Many studies using numerical simulation or observational analysis have suggested that Indian Ocean SST variations can modulate tropical Pacific SST changes (Wu and Kirtman 2004; Yu et al. 2002; Yu 2005; Kug et al. 2006; Ohba and Ueda 2007; Ohba and Watanabe 2012; Luo et al. 2010; Watanabe and Jin 2002; X. Wang et al. 2014; Peng et al. 2020). However, some SST anomalies in these studies may originally have been related to IOD modes instead of the whole basin mode, the Indian Ocean basin mode (IOB), which is the passive mode responding to ENSO forcing (e.g., Wu and Kirtman 2004; Kug et al. 2006; Kug and Kang 2006), as the numerical

Corresponding author: Wen Zhou, wenzhou@cityu.edu.hk

DOI: 10.1175/JCLI-D-20-0487.1

© 2021 American Meteorological Society. For information regarding reuse of this content and general copyright information, consult the AMS Copyright Policy (www.ametsoc.org/PUBSReuseLicenses).

experiments were usually designed to be coupled or uncoupled with the Indian Ocean without detailed discussion of SST patterns in the Indian Ocean.

Li and Li (2017) have defined a coupled mode of SST anomalies over the tropical Pacific–Indian Ocean in which the spatial pattern well reproduces the IOD–ENSO-associated SST pattern, and they also revealed its associated impacts on climate over Asia, the western Pacific, Africa, and even North and South America. These phenomena further imply a complex interaction and closely correlated relationship between ENSO and IOD modes. Therefore, it is necessary to reveal the interactive nature and mechanism of these two major climate modes before investigating their climatic and socioeconomic impacts.

While most previous studies have focused on the simultaneous interaction between ENSO and the IOD, which means the IOD and ENSO develop in the same year, few studies have viewed the interaction for a longer period. Izumo et al. (2010) proposed that the IOD can favor an opposite phase of ENSO with a lead of 1 year or so. They showed that when the IOD index is combined with warm water volume (WWV) in autumn to predict ENSO about 14 months later, the prediction skill score is significantly improved. Regarding the possible mechanism, they stated that a negative IOD with positive SST anomalies in the equatorial southeastern Indian Ocean can enhance the ascending branch of the Walker circulation and lead to easterly anomalies over the equatorial Pacific during autumn. Consequently, the sudden relaxation of easterly anomalies in winter along with the elimination of the IOD can lead to the development of El Niño the next year. The impacts of external IOD forcing on the Pacific Ocean are also examined in their subsequent study from an interdecadal perspective (Izumo et al. 2014). These studies focused particularly on improving prediction skill, but they paid limited attention to the detailed physical process of how the IOD influences the subsequent ENSO evolution. In their results, the zonal wind anomalies over the western equatorial Pacific associated with the IOD proved to be important for the development of the subsequent ENSO, suggesting the relatively dominant role of dynamic processes, although the role of thermodynamic processes in this relationship also needs examination. So in this study, a mixed layer heat budget analysis is conducted to examine the detailed physical processes, to reveal whether the role of dynamic processes is more important, and to determine the role of thermodynamic processes. By further inspecting the possible effect of the IOD on the following ENSO, we can better understand the interaction between the IOD and the subsequent ENSO, which will provide promising information for improving seasonal to interannual predictions of ENSO. This fresh perspective of the IOD leading ENSO could change the conventional notion that the IOD is a passive mode that is less important within the tropical Indo-Pacific Ocean and draw more attention to the possible impacts of the IOD on global climate with a longer lead time.

The organization of the text is as follows. Data and methodology used in this study are described in section 2. Section 3 investigates the simultaneous coupled relationship of ENSO–IOD and the IOD influences on the subsequent ENSO. A

discussion of how the Indian Ocean SST anomalies influence the zonal wind responses over the western Pacific in winter is given in section 4. Finally, a summary is given in section 5.

2. Data and methodology

a. Datasets

The monthly global Extended Reconstructed Sea Surface Temperature, version 5 (ERSSTv5), with a horizontal resolution of $2^\circ \times 2^\circ$ is employed in this study (Huang et al. 2017). Monthly ocean mixed layer depth, surface ocean net heat flux, ocean temperature, three-dimensional ocean current velocity, surface wind stress, and sea surface height (SSH) data from the Simple Ocean Data Assimilation (SODA), version 3.3.2, are utilized for the mixed layer heat budget analysis (Carton and Giese 2008). The ocean surface flux dataset is from the National Oceanography Centre, Southampton (NOCS), United Kingdom, version 2.0, containing monthly 1° gridded estimates of turbulent and radiative flux components along with the meteorological variables used in the flux calculation (Berry and Kent 2009, 2011). To analyze near-surface winds, horizontal winds at 10 m from ERA-Interim are adopted, with a resolution of $1^\circ \times 1^\circ$ (Dee et al. 2011). Outgoing longwave radiation (OLR) with a resolution of $2.5^\circ \times 2.5^\circ$ is used to denote the atmospheric heat source (sink) based on the High Resolution Infrared Radiation Sounder (HIRS) v2r2 (Lee et al. 2007). For a consistent investigation period, data from all the above datasets except heat flux from NOCS are selected from 1982 to 2017. As the NOCS v2.0 dataset provides data only before 2014, the investigation period is from 1982 to 2014.

b. Methodology

Boreal winter [December–February (DJF)]-averaged SST anomalies over the Niño-3.4 region (5°S – 5°N , 170° – 120°W) are taken as the Niño-3.4 index, considering that winter is usually the mature phase of ENSO (Rasmusson and Carpenter 1982). To represent IOD variation, the dipole mode index (DMI) during its mature phase [boreal autumn, September–November (SON)] is adopted; its definition, according to Saji et al. (1999), is the difference in SST anomalies between the western equatorial Indian Ocean (10°S – 10°N , 50° – 70°E) and the southeastern equatorial Indian Ocean (10°S – 0° , 90° – 110°E). In this study, an IOB index is also calculated based on area-averaged SST anomalies (10°S – 10°N , 50° – 90°E) during boreal spring [March–May (MAM)]. The correlation and regression analyses are calculated for seasonal fields with the representative indices for these two important climate modes to examine their influence. The partial correlation technique is also employed to extract the independent signals of the IOD from ENSO. Composite analysis is used to confirm the impacts of the IOD on the evolution patterns. The significance levels for the composite, correlation, and regression analyses are examined by the Student's *t* test.

To investigate the relative contributions of physical processes to the SST anomaly variations in the ensuing seasons after the IOD, a mixed layer heat budget analysis is conducted over the equatorial Indo-Pacific. Neglecting horizontal

diffusion, frictional heating, and interior oceanic turbulent heating, the heat budget equation within the mixed layer can be written as (He and Wu 2013):

$$\frac{\partial T}{\partial t} \approx \frac{Q_{\text{NET}}}{\rho C_p h} - \mathbf{V} \cdot \nabla T - w \frac{\partial T}{\partial z}, \quad (1)$$

where the $\overline{(\)}$ represents the vertical means of each parameter, calculated as

$$\overline{(\)} = \frac{1}{h} \int_{-h}^0 (\) dz. \quad (2)$$

The term T is the ocean mixed layer temperature, approximately represented by SST on the left side of the equation; Q_{NET} is the net surface heat flux; ρC_p is the specific heat capacity per unit volume, where the seawater density ρ is $1.029 \times 10^3 \text{ kg m}^{-3}$, and the specific heat capacity C_p is $3996 \text{ J kg}^{-1} \text{ K}^{-1}$; h is the mixed layer depth; \mathbf{V} is the horizontal ocean current; and w is the vertical current.

On the right side of Eq. (1), the first term embodies the net heat flux anomaly contribution, the second term is regarded as the oceanic horizontal advection contribution, and the third term represents the oceanic vertical process contribution. In the estimations for the terms on the right side, Q_{NET} , h , \mathbf{V} , and w are derived from the SODA dataset introduced earlier.

A series of numerical simulations are conducted in this study to examine wind responses over the tropical Indo-Pacific following IOD events, using a basic anomalous atmospheric general circulation model (AGCM) with five layers consisting of 0.1, 0.3, 0.5, 0.7, and 0.9 sigma levels, and a horizontal resolution of T42. This model has been utilized in many previous studies. For example, it has been used to investigate the effect of the mean state on modulating anomalous forcing in the tropical Indo-Pacific (Wang et al. 2003), to investigate the initiation of the boreal summer intraseasonal oscillation over the equatorial western IO (Jiang and Li 2005), to examine the effect of vertical shear on the summertime synoptic-scale wave train in the western North Pacific (Li 2006), and to study the modulation of the Pacific–Japan teleconnection on synoptic variability over the East Asia–western Pacific sector (Li et al. 2014). It is also reasonable to use it to investigate the influence of anomalous heating patterns related to ENSO on the climate (Leung et al. 2017).

3. Results

a. ENSO–IOD coupling mode

In the present study, the simultaneous coupled relationship between the IOD and ENSO from the autumn of the IOD peak to the summer of ENSO decay is examined using season-reliant EOF analysis (S-EOF). Figure 1 shows the seasonal evolution of the leading mode of SST anomalies over the tropical Indo-Pacific Ocean, which account for almost half of the total variance (46.1%). The spatial pattern is typical of the ENSO life cycle, with a positive center located in the central eastern Pacific, and negative values in the western Pacific. Meanwhile, the Indian Ocean also displays a typical IOD

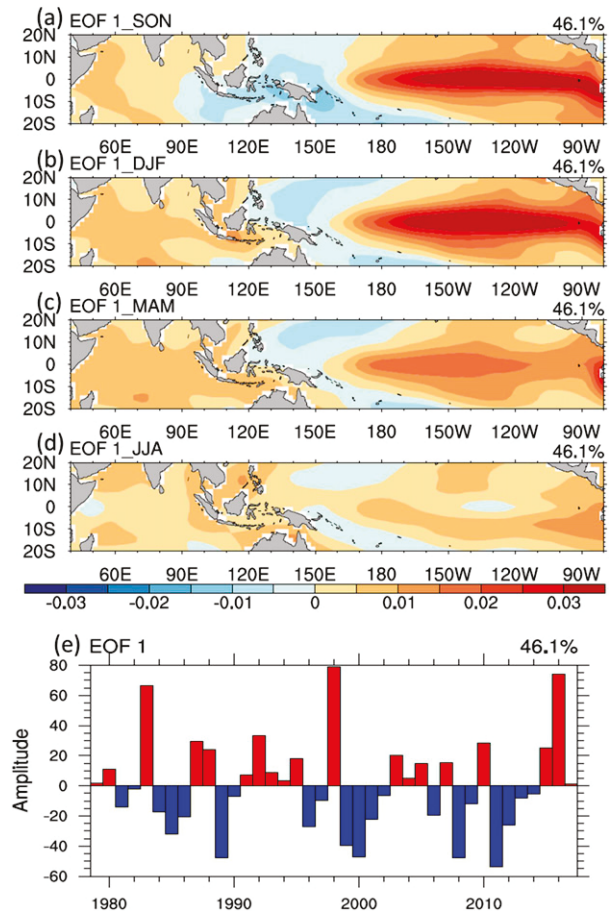


FIG. 1. (a)–(d) Seasonal evolution patterns of the first S-EOF mode based on ERSST v5 from 1981 to 2017 over the tropical Indo-Pacific Ocean. (e) Time series of the first principal component.

pattern during SON, which is an evident contrast between the eastern and western equatorial Indian Ocean, with weaker magnitudes compared to those in the Pacific. In the ensuing winter to summer (DJF to JJA), the SST pattern over the Indian Ocean is mainly a basinwide pattern (suggested as the IOB mode), which is a passive mode closely coupled with the ENSO cycle. The time series of the principal component of the first S-EOF mode is also plotted in Fig. 1e, where the temporal coefficients have large amplitudes in El Niño and La Niña years. The leading mode has a close association with the DJF Niño-3.4 index and the SON DMI, with a high correlation coefficient of 0.97 and 0.60, respectively. This indicates that this coupling mode is controlled mostly by the ENSO cycle, and the IOD oscillation is very likely to occur along with ENSO.

The seasonal evolution of SST anomalies with indices for ENSO and the IOD is also shown in Fig. 2. The dotted region here denotes correlation coefficients significant at the 90% confidence level according to the Student's t test. Based on correlation maps with the Niño-3.4 index, anomalous warming SST dominates the equatorial central and eastern Pacific associated with the positive phase of ENSO events (El Niño), while anomalous cooling SST is obvious over the western

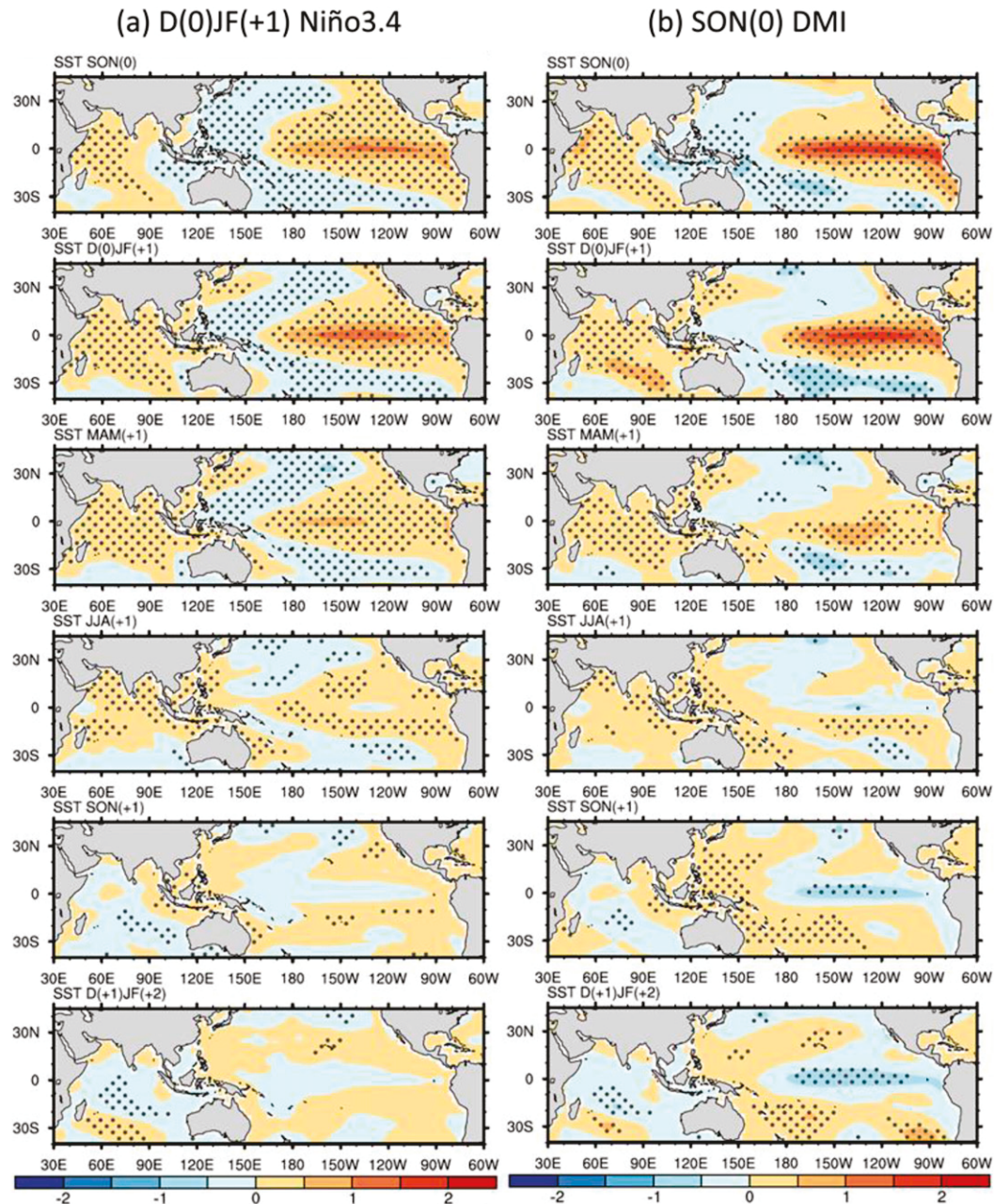


FIG. 2. Regressions of seasonal SST anomaly evolution on the (a) Niño-3.4 index in D(0)JF(+1) and (b) DMI in SON(0). Dotted areas are statistically significant at the 90% confidence level. The numbers 0, +1, and +2 in parentheses indicate that the month belongs to the same year, the ensuing year, or the year after the ensuing year of IOD events, respectively.

Pacific and the southeastern Indian Ocean during the developing autumn of ENSO [SON(0); Fig. 2a]. During the ensuing winter, ENSO reaches its peak and the IOD-like pattern deteriorates in the equatorial Indian Ocean. In MAM(+1), the ENSO pattern shows a decaying trend in the Pacific, and a basin warming pattern over the Indian Ocean lasts until the ensuing summer. These evolution patterns basically reproduce the leading mode distribution in the S-EOF results (Fig. 1),

confirming that the ENSO–IOD coupling mode is dominated by the ENSO cycle. It is worth noting that ENSO continues to decay in the following seasons, and there is almost no obvious signal over the Pacific during the next winter.

When the DMI is used for correlation analysis (Fig. 2b), the evolution of the SST field shows a similar pattern from the simultaneous autumn to the ensuing spring, illustrating the ENSO decay in the Pacific and the shift from the IOD to IOB

in the Indian Ocean. However, the difference in the SST evolution process associated with the IOD and ENSO appears after the ensuing summer, where following the IOD cases, significant negative values occur after the ensuing summer over the equatorial central and eastern Pacific. With time, these negative SST signals persist and grow into a La Niña-like pattern the next winter. This tendency is indeed noteworthy, as it may indicate that the IOD can favor phase changes of ENSO and provide promising information for the prediction of ENSO with a 1-yr lead time. Moreover, the out-of-phase leading relationship of the IOD with the subsequent ENSO has been indicated in Izumo's work (Izumo 2010), which found that IOD events can make significant contributions to the forecast of ENSO with a 1-yr lead. Regarding the mechanism, they proposed that the sudden relaxation of a negative IOD can trigger zonal wind anomalies over the western Pacific and influence the evolution of the subsequent ENSO, as mentioned in the introduction. However, in their study, this explanation was given without a detailed examination of each process. So in the following section, we want to examine in detail how the IOD influences the following ENSO evolution and revisit the possible role of the IOD in the development of ENSO.

b. Possible favorable role of the IOD in the development of ENSO

To identify the role of the IOD in the following ENSO, a partial correlation analysis between SST anomalies and the DMI is conducted to remove the linear influence of ENSO, as shown in Fig. 3. During autumn (Fig. 3a), the typical SST contrast between the eastern and western equatorial Indian Ocean is evident, while positive anomalies can also be observed over the equatorial eastern Pacific, indicating that even after removal of the linear relationship with the Niño-3.4 index in winter, significant simultaneous signals over the far eastern equatorial Pacific are still evident. During the ensuing winter (Fig. 3b), the cold pole of the IOD deteriorates and the warm pole weakens in the Indian Ocean; in addition, positive values shrink in the eastern Pacific but cooling values are obvious in the central portion, which is the major distinction compared to the regression results and indicates the cooling effect of the IOD on Pacific SST. After the ensuing spring, the signals over the Indian Ocean become insignificant, while the negative values over the central Pacific are still significant and can strengthen with time, lasting until the next winter (Figs. 3c–f). The negative SST signals in the next winter indicate that a La Niña event manages to occur following the IOD in the last year.

Since the comparison of regression analysis with the DMI and Niño-3.4 index in Fig. 2 reveals that the SST evolution patterns associated with the Niño-3.4 index fail to display the phase-changing pattern from the first winter to the next, it is reasonable to state that the ENSO cycle itself does not have a stable biennial oscillation. Therefore, the SST cooling process associated with the IOD cannot be seen as an intrinsic oscillation related to the coupled ENSO cycle. To further exclude this possibility, the monthly correlation coefficients between the Niño-3.4 index and autumn DMI in the first year are calculated in Fig. 4a. Compared with the monthly autocorrelation

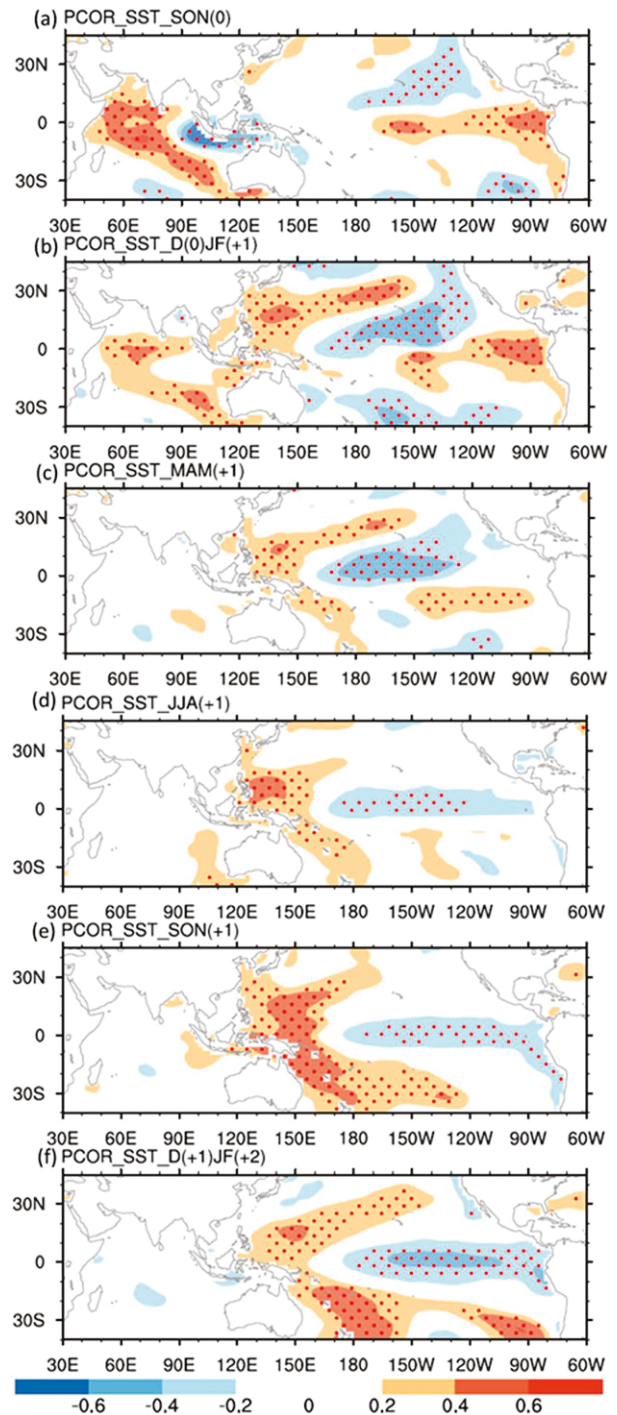


FIG. 3. Partial correlation of seasonal SST anomaly evolution on DMI independent of Niño-3.4. Dotted areas are statistically significant at the 90% confidence level. The numbers 0, +1, and +2 in parentheses indicate that the month belongs to the same year, the ensuing year, or the year after the ensuing year of IOD events, respectively.

between the Niño-3.4 index and its value in the first winter (Fig. 4b), ENSO itself does not display a phase-changing tendency, and the sudden drop after spring confirms the “spring prediction barrier” phenomenon (Webster and Yang 1992).

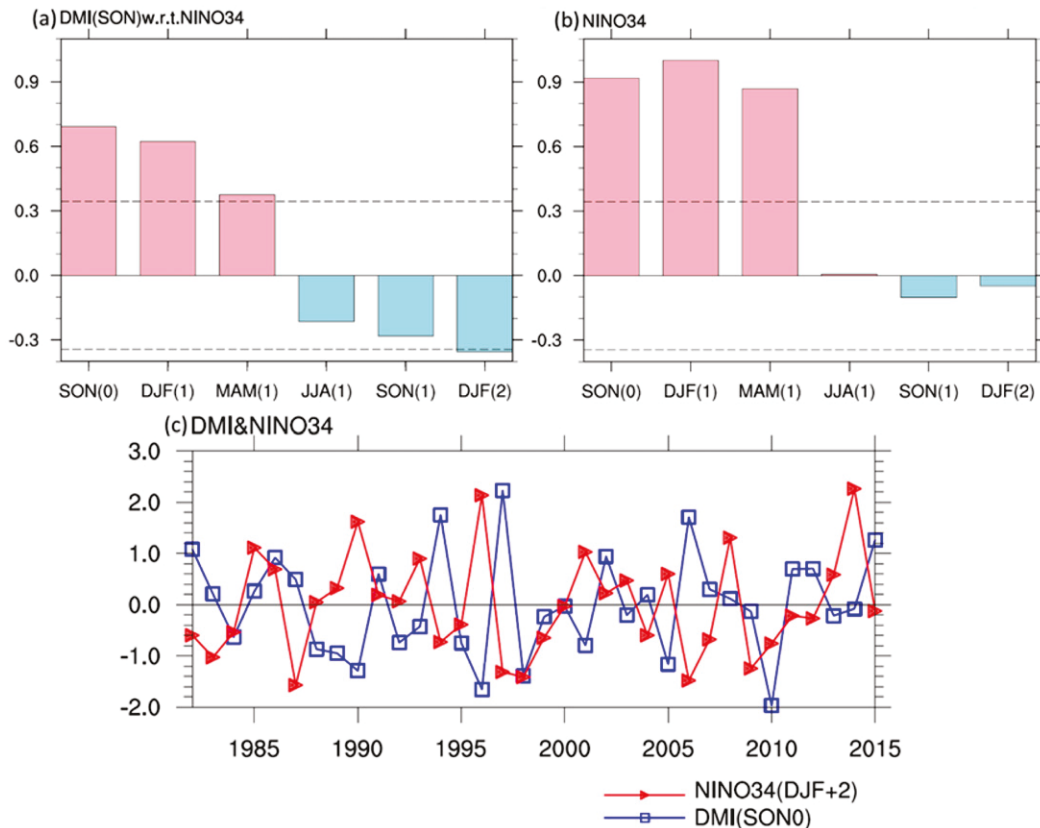


FIG. 4. Lead-lag partial correlation coefficients of seasonal Niño-3.4 with (a) DMI in autumn (SON) and (b) Niño-3.4 in winter [DJF(1)]. Dashed lines denote the correlation coefficients at the 90% significance level. The numbers 0, +1, and +2 in parentheses indicate that the month belongs to the same year, the ensuing year, or the year after the ensuing year of IOD events, respectively. (c) Time series of DMI in autumn and Niño-3.4 of the next winter.

Given the time series of the DMI in the first autumn and the Niño-3.4 index in the next winter, shown in Fig. 4c, the correlation between the Niño-3.4 and the DMI with a 1-yr lead is also calculated as -0.37 , significant at the 95% confidence level. These results suggest a possible favorable role of the IOD in the development of the ensuing ENSO, which supports Izumo's statement and is worth further investigation (Izumo et al. 2010).

c. Mixed layer heat budget analysis associated with IOD forcing

A mixed layer heat budget analysis is conducted to reveal how the IOD can lead to an SST response over the equatorial Pacific. According to Eq. (1), the SST change is influenced largely by changes in dynamic ocean processes (advection and upwelling) and net heat flux. The terms in the heat budget analysis equation are first calculated, and consequently the partial correlation coefficient of evolution with regard to the DMI in the IOD peak season after removing the IOB index during spring is analyzed to identify the role of the IOD in the subsequent ENSO. The reason for separating the IOD from the IOB is that there is still controversy among previous studies about whether the mechanism of the IOD's influence on

ENSO in the subsequent year is independent of the IOB (e.g., Annamalai et al. 2005; Dayan et al. 2014). On the other hand, given the strong simultaneous associations between the IOB and ENSO, removing the IOB influence when investigating the IOD modulations can also approximately offset the influence of ENSO.

The partial correlation results show that, led by a positive IOD case, the SST cooling tendency is dominant over the equatorial central and western Pacific after autumn (Fig. 5a). The SST cooling tendency denotes that the IOD can cool down the SST over the Pacific and may lead to a phase change of ENSO. The contributions of different parameters to the SST tendency are also investigated based on the correlated evolution process of net heat flux anomalies, ocean advection anomalies, and ocean upwelling departure for more than 1 year after the peak season of an IOD event. In the ensuing winter and spring, the contribution from net heat flux to SST cooling is most important (Fig. 5b), which may be due mainly to the negative cloud-radiation-SST feedback. The SST warming related to the simultaneous coupled El Niño would enhance in situ convection, thus increasing cloudiness and reducing solar radiation. The cooling SST tendency over the Pacific reaches its maximum during the ensuing winter and spring, and

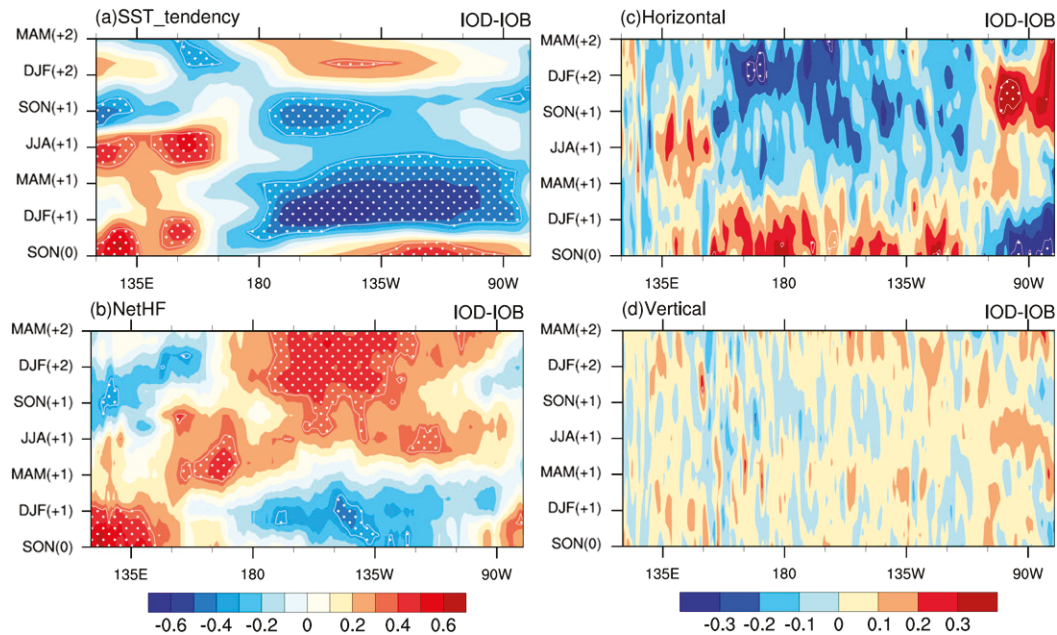


FIG. 5. Partial correlation of 3-month moving average of (a) SST tendency, (b) net heat flux, (c) oceanic advection, and (d) ocean upwelling on DMI in autumn [SON(0)] after removing the linear relationship with IOB index in spring [MAM(+1)]. Dotted areas are statistically significant at the 90% confidence level.

then it shrinks and is confined to the central Pacific and lasts until early the next winter. After the ensuing spring [MAM(+1)], the dominant contributing term changes to oceanic horizontal advection, with the maximum negative contribution first developed over the central Pacific (Fig. 5c), which is also the reason that after this spring, the SST cooling tendency center shifts to the central Pacific. Oceanic horizontal processes help the SST cooling tendency evolve into a cold phase of ENSO the next year, while the atmospheric impacts on the ocean are mostly to increase the downward net heat flux and undermine the SST cooling process after MAM(+1). Nonetheless, it may be noticed that during the later stage, the significance of a single parameter is not as strong as the SST cooling tendency, and the cooling tendency is possibly related to some neglected terms in the heat budget analysis equation as well, such as the horizontal and vertical diffusion processes.

Based on the DMI in autumn exceeding 0.7 standard deviation, positive and negative IOD years are identified and listed in Table 1. The simultaneous ENSO and the subsequent ENSO conditions are also given in Table 1. The positive IOD cases have a better coupling relationship with the simultaneous El Niño, while negative IOD cases occur with the neutral phase of ENSO or La Niña. For the subsequent ENSO, positive IOD cases tend to lead to neutral or La Niña cases, and negative ones tend to lead to neutral or El Niño cases. So either way, a cooling SST tendency is expected to occur following a positive IOD, and a warming SST tendency is likely following a negative IOD. To further confirm the signals of the SST evolution, the SST and its tendency evolution are investigated via composite analysis with a focus on positive IOD cases (Fig. 6). To show their evolution associated with the mature phase of the

IOD, we show the distribution from SON(0) to three seasons later, in JJA(+1). During the IOD mature phase, SON(0), the prominent features related to the IOD and El Niño are obvious over the tropics. During the mature phase of the coupling ENSO, basinwide warming is observed in the tropical Indian Ocean, and the El Niño pattern persists in the equatorial central and eastern Pacific. These patterns again confirm the simultaneous coupling relationship between the IOD and ENSO. After winter, the El Niño signals deteriorate over the Pacific, and an anomalous cooling SST maximum occurs over the equatorial central Pacific. The SST tendency evolution amplifies the SST response to the IOD, where there are strong negative signals over the equatorial central-eastern Pacific following the IOD cases from winter, suggesting that the IOD may be beneficial to the rapid elimination of ENSO and to the initiation of opposite ENSO events.

The evolution of different parameters in the heat budget equation over the equatorial Pacific is also calculated based on a composite of positive IOD cases (Fig. 7), which basically reveals characteristics similar to Fig. 5. To further investigate the contributions of different terms in the heat budget equation over different Niño regions with a focus on positive IOD cases, the regional mean situation is further examined by composite

TABLE 1. Years of positive and negative IOD; definitions according to DMI. Simultaneous ENSO years boldfaced; subsequent ENSO years italicized.

Positive IOD	1982, 1994, 1997, 2002, 2006, 2015
Negative IOD	1989, 1992, <i>1996, 1998, 2010, 2014</i>

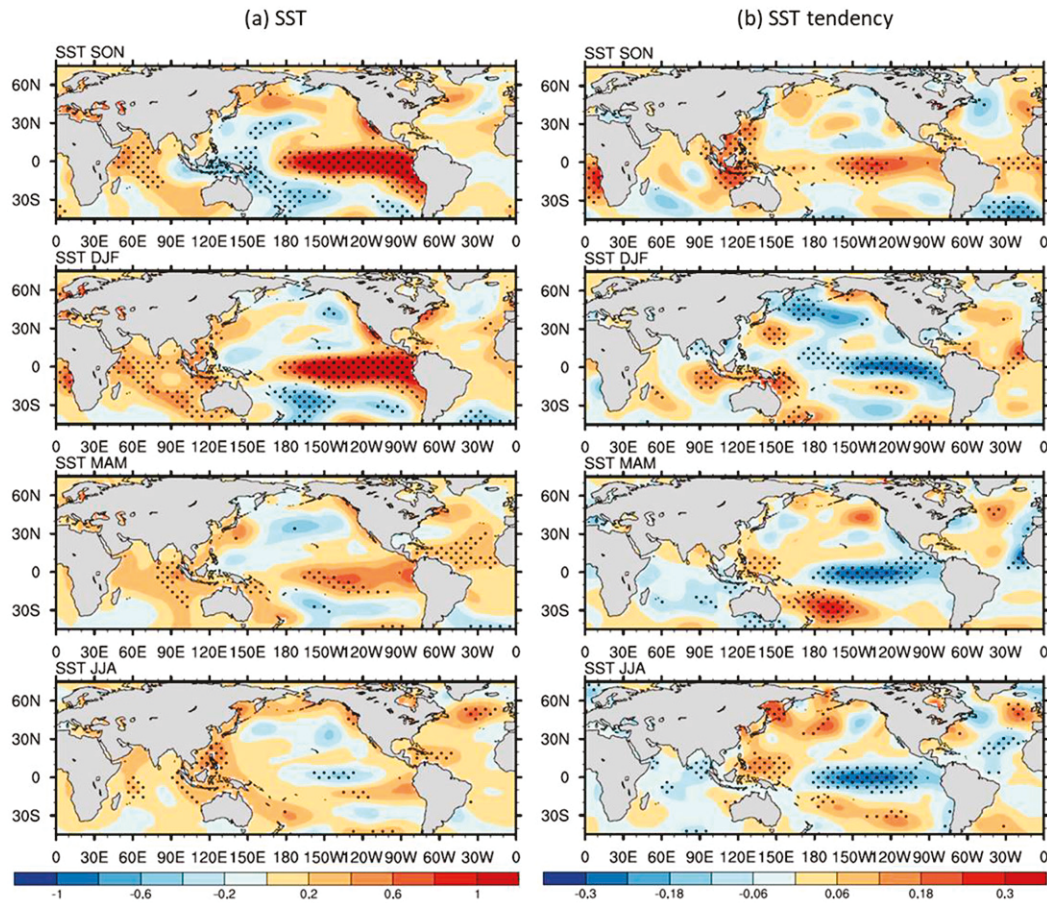


FIG. 6. Composite based on positive IOD cases of (a) seasonal SST anomalies ($^{\circ}\text{C}$) and (b) SST tendency anomalies ($^{\circ}\text{C}$). Dotted areas are statistically significant at the 90% confidence level.

analysis (Fig. 8). Generally, both the Niño-3 and Niño-4 regions show an SST cooling tendency following a positive IOD, as well as a transition of the dominant role from the net heat budget to oceanic processes around late spring. In more detail, over the Niño-3 region, before MAM(+1) the net heat flux dominates the SST cooling, as it reaches a maximum of $-5 \times 10^{-7} \text{ K s}^{-1}$, which is much larger than the SST tendency. However, after spring, the net heat flux becomes positive and tends to lead to SST warming instead. Vertical oceanic processes contribute to the SST cooling year round, and horizontal oceanic advection starts to contribute to the SST cooling after the ensuing spring [MAM(+1)]. In the Niño-4 region, the basic process is similar to the situation described earlier, while the contribution of horizontal oceanic advection plays a more important role in modulating the SST changes in that it tends to have the greatest magnitude of all the parameters. Before MAM(+1), some other oceanic process must cancel the effect of the horizontal advection in order to display the magnitudes of the SST cooling trend, while after the ensuing spring, the considerable magnitude of horizontal advection can certainly dominate the SST cooling tendency. These results are generally consistent with those of previous studies, although the primary focus is mainly on the ENSO life cycle, but we can find

similar patterns in these studies using different ocean reanalysis datasets (e.g., Santoso et al. 2017; Kim et al. 2015).

To fully clarify the contributions of thermodynamic processes to changing SST after the IOD cases, the different components of net heat flux are also investigated. Net heat flux should include net shortwave radiation, net longwave radiation, latent heat flux, and sensible heat flux. The evolution of the partial correlation coefficients of these terms associated with the IOD is given in Fig. 9. The two most important terms are the shortwave (SW) and longwave (LW) radiation flux based on the results without considering magnitude. But as we know, the magnitude of downward net longwave radiation is very limited, so the significant correlation suggests only that its variation has a close passive relation with the preceding IOD forcing. These results indicate that the IOD can influence the atmosphere and the cloudiness above the equatorial Pacific, hence modulating the downward longwave and shortwave flux into the ocean. Moreover, the contribution of latent heat flux (LHF) is significantly correlated to the preceding IOD event, as shown by the downward LHF decreasing from SON(0) to JJA(+1), benefiting the cooling tendency of SST over the Pacific. Meanwhile, it can also be seen that sensible heat flux can contribute to a decrease in SST during the ensuing spring

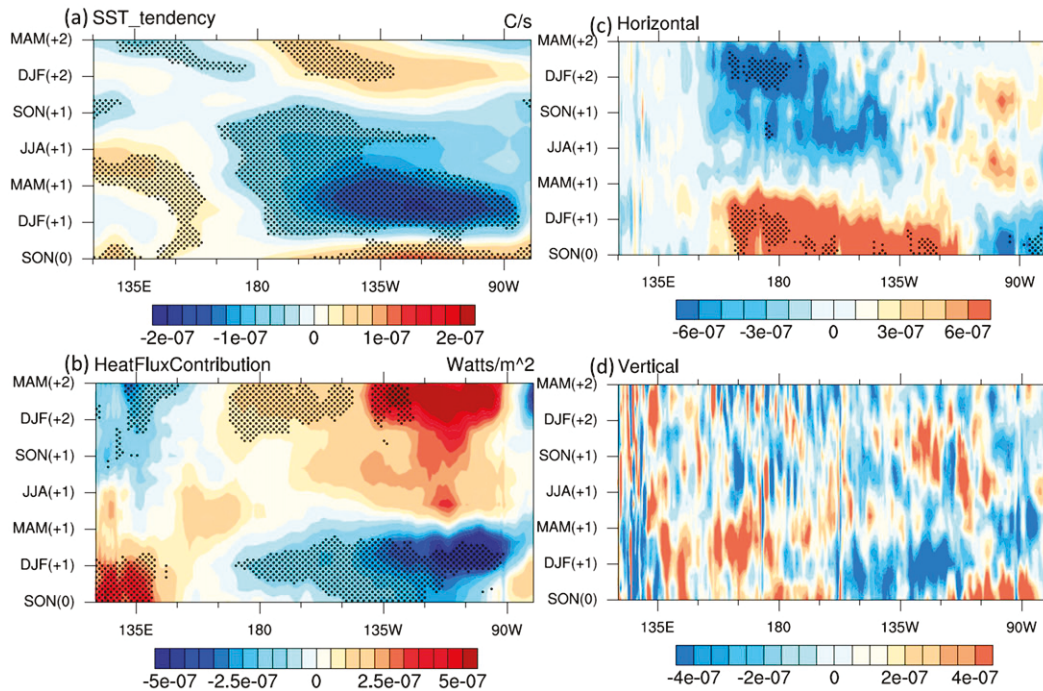


FIG. 7. Composite based on positive IOD cases of seasonal (a) SST tendency, (b) net heat flux, (c) oceanic advection, and (d) ocean upwelling. Dotted areas are statistically significant at the 90% confidence level.

and summer. Composite analysis based on positive IOD cases is also performed to compare the different components of net heat flux (Fig. 10). The results are similar to those shown in Fig. 9, further supporting the dominant roles of SW and LHF in net heat flux. These two terms are closely related to the variation in convection and surface wind in the atmosphere.

d. Possible mechanisms

1) CLOUD–RADIATION AND WIND–EVAPORATION–SST FEEDBACK

Based on the above analysis, the turning point of the evolution process associated with the IOD can be identified as the ensuing spring after the IOD. Before this spring, the SST tendency is controlled by changes in net heat flux, while after this spring, it is dominated by oceanic processes, especially horizontal advection. The focus of the following discussion is the first stage, from SON(0) to MAM(+1), when net heat flux contributes the most to the SST cooling tendency. Atmospheric forcing should at first come primarily from cloud–radiation effects, as indicated by the response of SW over the Pacific (Fig. 9d).

Nonetheless, after DJF(+1) the wind–evaporation–SST feedback should be more important for the Pacific, as indicated by the LHF response (Fig. 9a). To show that the wind–evaporation–SST feedback can explain the SST evolution in the following months, partial correlation analysis is also conducted on zonal and meridional surface winds and wind speed with regard to the DMI in the mature season of the IOD. Following the IOD cases, the northerly winds prevailing over the whole Pacific meridionally and the zonal alternation from westerlies to easterlies gradually occurring from the western to

the eastern Pacific can be observed in Figs. 11a and 11b. By comparing to the climatological seasonal changes in surface winds over the Pacific (Figs. 11c,d), we can deduce that the meridional wind response is favorable for increasing wind

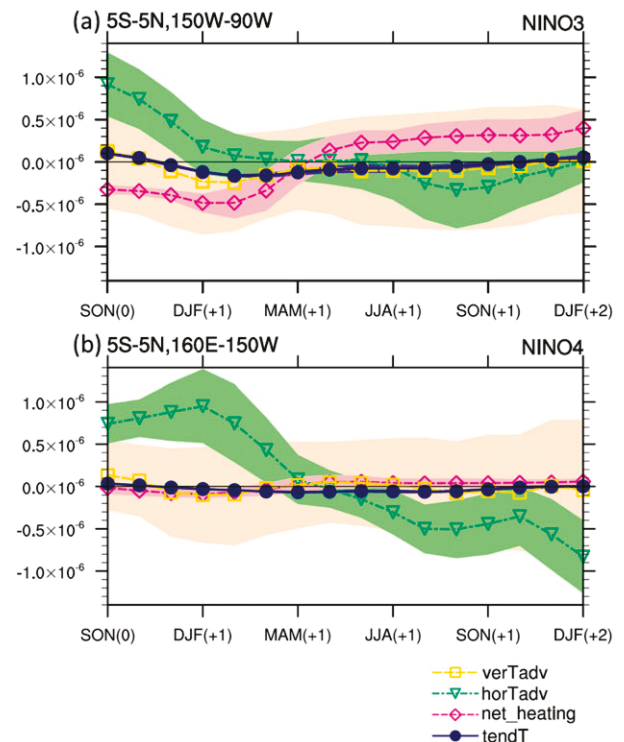


FIG. 8. Composite based on positive IOD cases of regional averaged mixed layer budget analysis. Error bars with one standard error of the mean above and below the means are given.

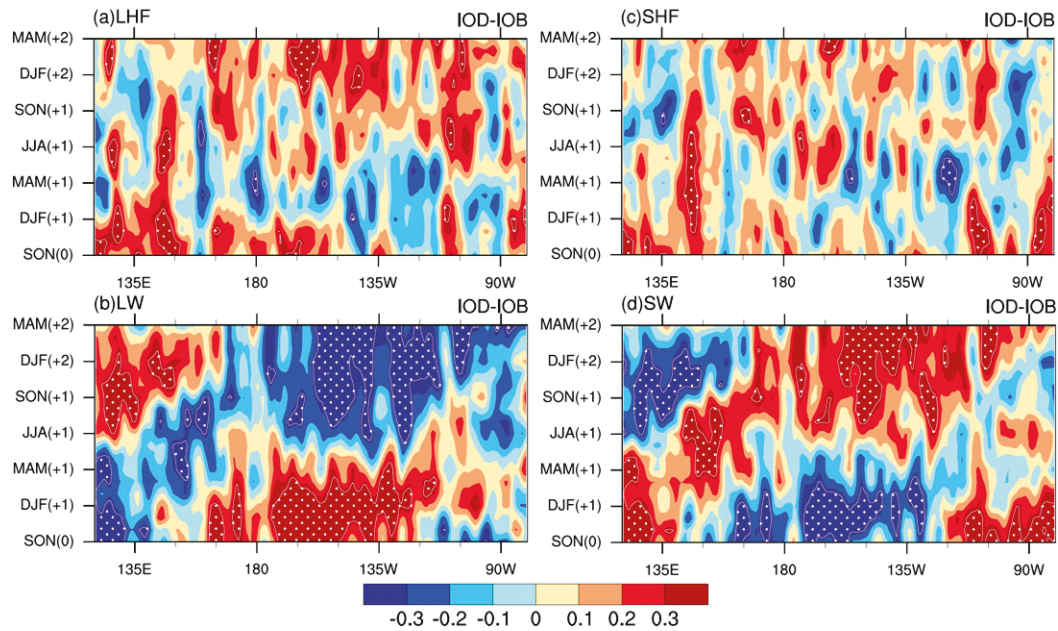


FIG. 9. As in Fig. 5, but with different downward components of surface net heat flux.

speed over the central Pacific during winter, and the zonal easterly response should cause a velocity increase as well. These modulation effects can be confirmed in the wind speed evolution pattern in Fig. 11e, whose positive values are mainly consistent with the evolution of the easterly response (Fig. 11a). Starting from the ensuing winter, to the west of 120°W, increasing wind speed is evident, and the decreasing release of latent heat to the atmosphere is also obvious in this

region (Fig. 9a), which indicates that the wind–evaporation–SST feedback is contributing to the SST cooling tendency for the equatorial Pacific from DJF(+1) to MAM(+1).

2) BJERKNES FEEDBACK

The mechanism by which the IOD favors the development of the subsequent ENSO after the ensuing spring is also discussed in this study. According to the mixed layer heat budget

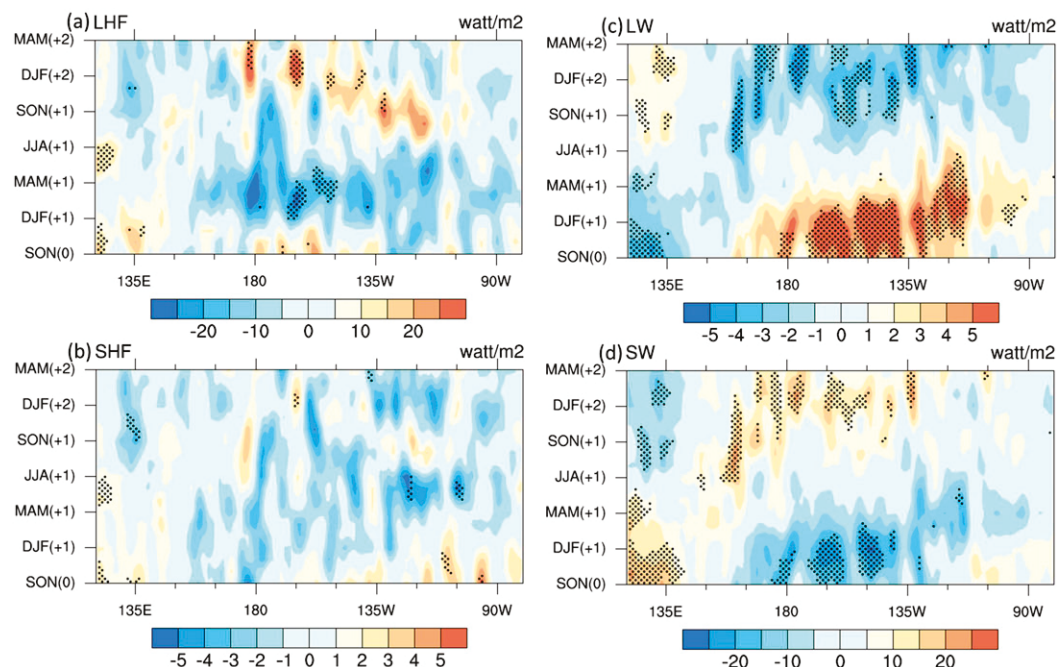


FIG. 10. As in Fig. 7, but with different downward components of surface net heat flux.

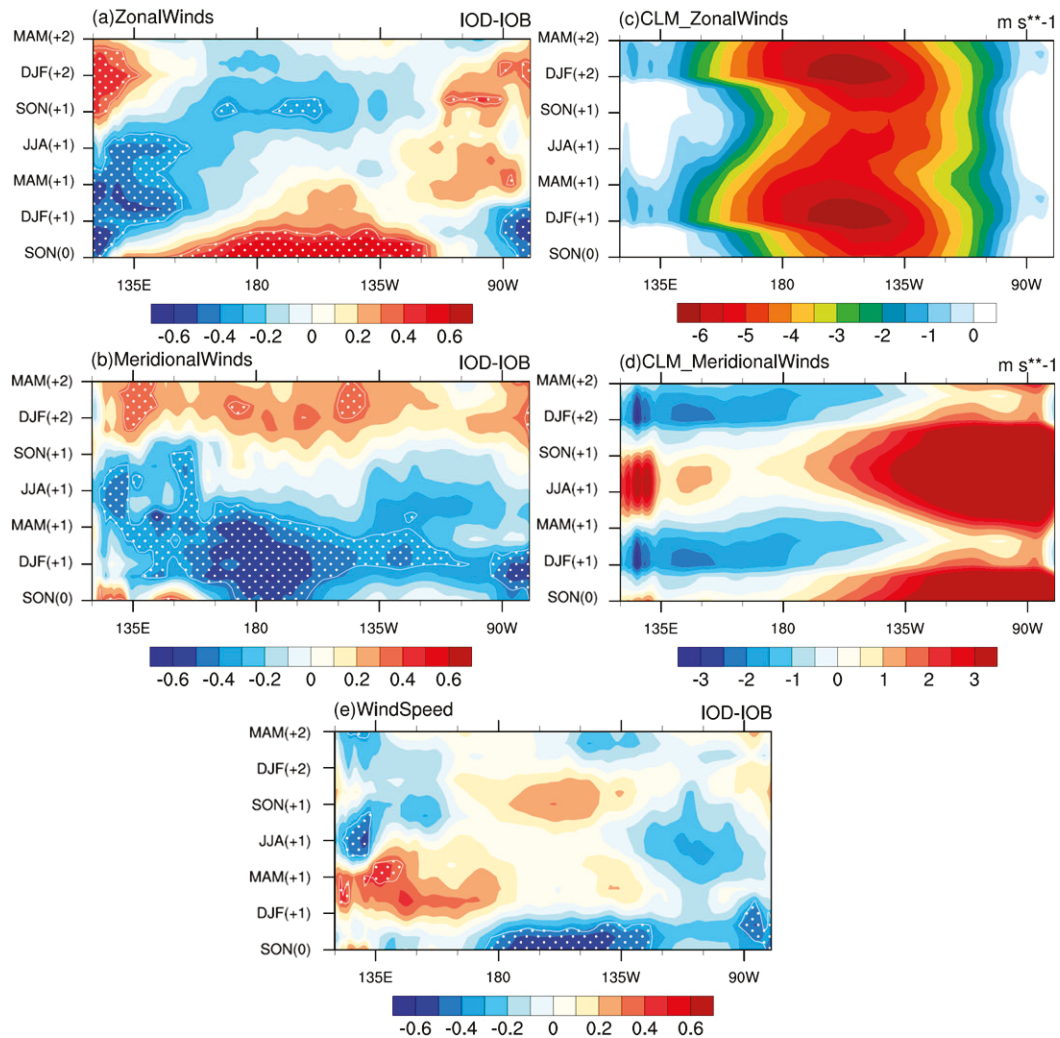


FIG. 11. Partial correlation of 3-month moving average (a) zonal wind anomalies, (b) meridional wind anomalies, and (e) wind speed anomalies on DMI in autumn [SON(0)] after removing the linear relationship with IOB index. Dotted areas are statistically significant at the 90% confidence level. Climatological evolution of (c) zonal winds, and (d) meridional winds.

analysis, after the ensuing spring, horizontal oceanic advection starts to contribute to the SST cooling tendency, which can persist for several months to the next year (Figs. 5c and 7c). In addition, vertical motion also appears to contribute to the SST cooling after the ensuing spring over the equatorial central Pacific (Figs. 5d and 7d). These signals suggest that oceanic processes are most important in maintaining the SST cooling tendency, especially in the central Pacific. This is probably due to the local Bjerknes feedback becoming stronger during this period.

After spring, in the zonal wind field, easterlies prevail over the equatorial western and central Pacific, as shown in Fig. 11a. Along with the zonal wind evolution, the zonal wind stress anomaly field (Fig. 12c) shows a similar process: westward anomalies develop from the western Pacific and propagate

eastward, while eastward anomalies are significant after spring east of 120°W. Responding to the wind stress anomalies, oceanic divergence can be expected over the central Pacific, which may lead to a lift in the thermocline. In this study, we plot SSH to approximately represent the variation in the thermocline, as illustrated in Fig. 12b. The thermocline evolution shows an eastward-propagating negative response to the preceding IOD, where the maximum is located over the central Pacific after the ensuing spring as expected. This pattern agrees with the location of the maximum SST cooling tendency (Fig. 5a). As a result, the interaction between equatorial zonal wind and thermocline depth can lead to the SST cooling response (Fig. 12a), which together can be considered as a local Bjerknes feedback for the Pacific contributing to the formation of a La Niña-like pattern the next winter.

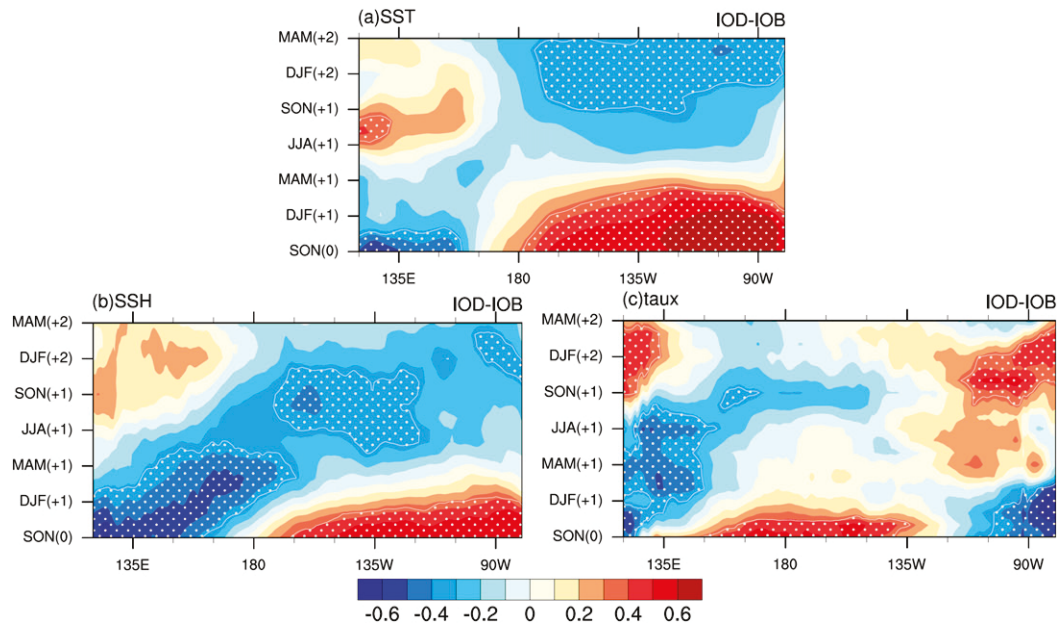


FIG. 12. As in Fig. 5, but with (a) SST anomalies, (b) SSH anomalies, and (c) zonal wind stress.

4. Discussion

The results discussed in this study support most of the assumptions in Izumo et al. (2014, 2010). It is also noteworthy that they stated that the effect of the IOD on the initiation of the subsequent ENSO requires preconditioning by the Pacific WWV. Regarding the role of WWV, our results reveal thermocline shoals responding to the IOD forcing in the equatorial central and eastern Pacific, indicating a decrease in WWV. These phenomena imply that the decrease in WWV is also likely attributable to the preceding positive IOD forcing; meanwhile, the decreasing WWV will also contribute to the development of La Niña.

Meanwhile, the importance of the wind response in the western Pacific has also been revealed in this study. Whether it is early wind–evaporation–SST feedback or late Bjerknes feedback, the zonal wind response plays a leading role. However, why the IOD can trigger the zonal wind responses after its demise is a complex question that has not been fully answered. Izumo et al. (2016) have revealed that some portion of zonal wind responses in the ensuing seasons over the western equatorial Pacific associated with IOD forcing can be explained by its effect on the amplification of IOB impacts. Zhang et al. (2019a) proposed a mechanism to explain why the IOD can exert a delayed influence on Asian climate, which is that the IOD can increase the snowpack on the southern Tibetan Plateau in early winter, and the excessive snowmelt induces a decrease in the meridional land–sea thermal contrast and easterly anomalies in the equatorial Indian Ocean and western Pacific. Previous work has deeply investigated the wind response related to Indian Ocean SST anomalies associated with ENSO, confirming that during the winter, even though the IOD mode has already disappeared, the atmospheric heat remains in a dipole pattern (Chen et al. 2016),

while the heat sink over the eastern equatorial Indian Ocean should lead to westerlies over the western Pacific. In that case, it is difficult to understand how the easterly anomalies are evident in observations (e.g., Wang et al. 2000; Wu et al. 2009b; Li et al. 2017) and this study. To investigate the wind response in the western Pacific, the anomalous AGCM model is adopted to simulate the influence of the anomalous heating pattern in the Indian Ocean on the winter climate over the Indo-Pacific. The dipole heating pattern in winter is based on the composite OLR field of positive IOD cases (Fig. 13b), which are prescribed in the simulations as the green contours in Fig. 14. The OLR pattern indeed shows that when the IOD decays in the ensuing winter, the heating pattern in situ still persists as a dipole mode. However, the heat sink center over the eastern Indian Ocean is located more northward and over the Bay of Bengal. Results of simulation with the dipole heating pattern are shown in Fig. 14a, which demonstrates that although the heat sink is evident, the easterlies are the resultant wind

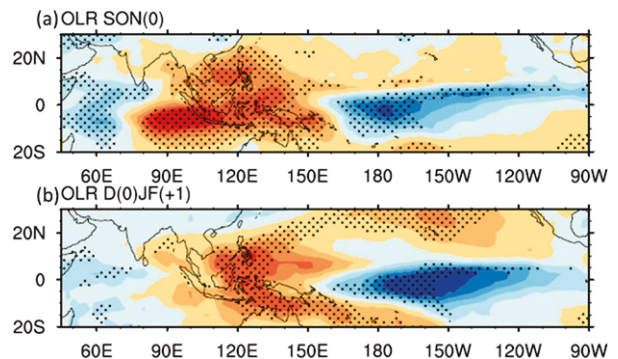


FIG. 13. As in Fig. 6, but with OLR fields.

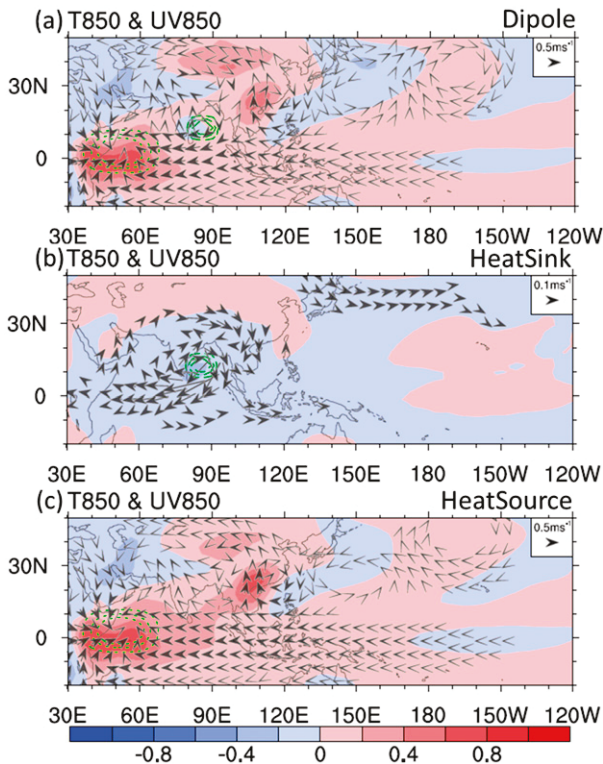


FIG. 14. (a)–(c) 850 hPa air temperature anomalies (K) and horizontal wind anomalies [vectors; showing only magnitude $> 0.1 \text{ m s}^{-1}$ in (a) and (c) and magnitude $> 0.02 \text{ m s}^{-1}$ in (b)] in response to anomalous heat pattern using a linearized anomalous AGCM prescribing the DJF climatology. Green contours represent heat sources (sinks) at the 0.5 sigma level with an interval of 0.2 K day^{-1} .

response over the Pacific. To further investigate the reason for this, we also conducted separate simulations with only the heat sink or the heat source. With only the heat sink in the eastern Indian Ocean, the weak westerlies are triggered over the western Pacific and Maritime Continent (Fig. 14b). However, the heat source is much larger in the western Indian Ocean (Fig. 13b), which can trigger a massive Rossby wave response as a Gill-type response in the simulation, and strong equatorial easterlies ranging from the Indian Ocean to the Pacific (Fig. 14c). As a result, when both heat poles are added in the simulation, the easterlies still dominate the western equatorial Pacific. So these simulation results confirm that although the dipole heat pattern still exists after the demise of the IOD, the warming pole in the western Indian Ocean is much stronger and dominant, so under its influence, the easterlies are the resultant response in the western equatorial Pacific.

Another important issue in this study is related to the relative contributions of the IOD and IOB. Some previous work has argued that the effect of the IOD is not as dominant as that of the IOB on the evolution of the subsequent ENSO (e.g., Annamalai et al. 2005). To compare their effect, partial correlations of terms in the heat budget equation with the IOB index after removing the influence of the IOD are also

analyzed. Revealed by the SST tendency signals (Fig. 15a), the IOB mode can also lead to an SST cooling trend over the equatorial Pacific, which agrees well with some previous work (Kug et al. 2006; Kug and Kang 2006; Ohba and Ueda 2007; Yamanaka et al. 2009). Compared to the effect of the IOD (Fig. 5a), the persistence of cooling SST tendency responses is relatively shorter, ending before the autumn in the subsequent year [SON(+1)]. Considering that the IOB is very likely to co-occur with an ENSO case over the equatorial Pacific, such a phenomenon indicates that the IOB mainly speeds up the decay of the simultaneous ENSO event, while the unique role of the IOD is to favor the initiation of the subsequent ENSO. During the ENSO decay seasons, the dominant processes associated with IOB cases are net heat flux and vertical oceanic processes. The former dominant process is the same as that associated with IOD forcing, also implying that cloud–radiation–SST feedback contributes the most to the SST cooling tendency. As for the latter, the IOB has a distinctive role in triggering ocean upwelling over the central and western equatorial Pacific, leading to the SST cooling pattern. A difference is also identified in oceanic horizontal processes, which occur during the same period and primarily hamper the SST cooling trend, offsetting the other two processes over the western and central Pacific.

5. Summary

In the present study, the interaction between the IOD and ENSO is investigated deeply with a special focus on IOD impacts on the ensuing ENSO. The simultaneous coupled relationship between ENSO and the IOD is first examined, using 0 to denote the year when a coupled ENSO and IOD occur together, showing that along with the ENSO(0) cycle, the typical IOD pattern is obvious in the equatorial Indian Ocean during autumn. Regression analysis reveals that IOD-related evolution has some difference with the ENSO-related pattern, where negative signals dominate the equatorial central and eastern Pacific. These patterns persist and grow into a La Niña-like pattern the next winter, indicating a possible role of the IOD in the subsequent ENSO.

Consequently, the abovementioned possible impacts of the IOD on ENSO are further investigated by conducting partial correlation analysis between SST and the DMI after removing the influence of ENSO, which shows evolution characteristics similar to those of the regression results. The autocorrelation of the Niño-3.4 index does not show the stability of the ENSO biennial oscillation, clarifying that the significant responses of SST evolution in the ensuing year associated with IOD forcing are not likely related to the ENSO oscillation by itself.

A mixed layer heat budget analysis is utilized to examine the detailed process of how the IOD influences the ENSO life cycle in the next year [herein ENSO(+1) refers to the subsequent ENSO] and to compare the different roles of dynamic (wind forcing) and thermodynamic (heat flux) processes in inducing the SST changes over the Pacific. Correlation and composite results confirm that following the IOD the SST cooling tendency is evident over the equatorial central and western Pacific and can last for more than one year, benefiting

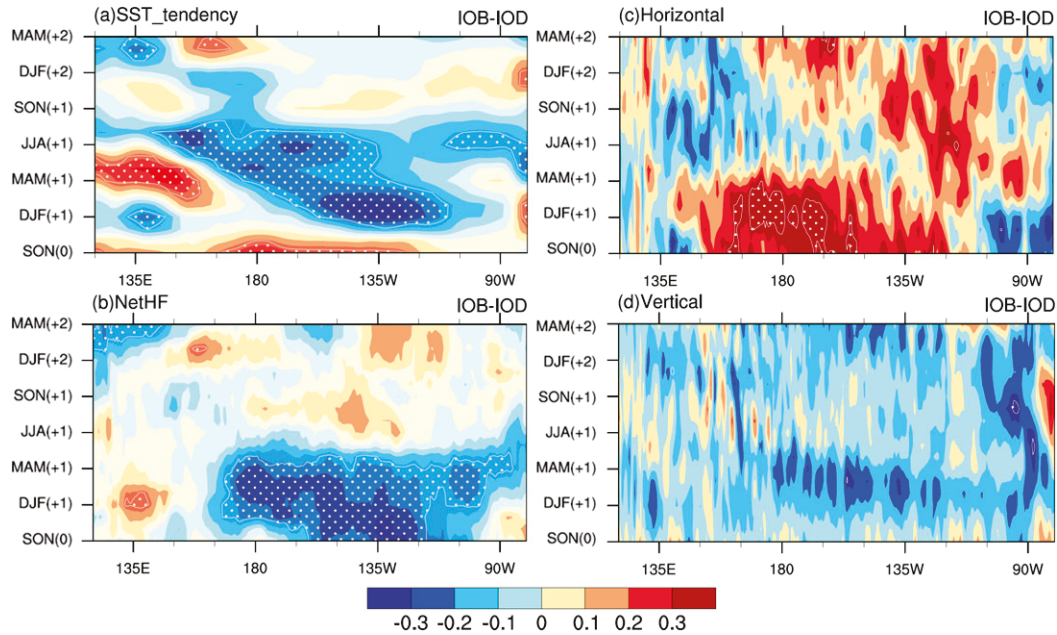


FIG. 15. As in Fig. 5, but with regard to IOB index in the spring [MAM(+1)] after removing the linear relationship with DMI in the autumn [SON(0)].

the development of the subsequent ENSO event. The SST cooling tendency associated with a positive IOD is contributed primarily by net heat flux from autumn to the ensuing spring [MAM(+1)]. After the ensuing spring [MAM(+1)] the dominant contribution comes from oceanic processes instead, with a maximum negative contribution over the central Pacific. The regional heat budget analysis comparing the Niño-3 and Niño-4 regions reveals that before MAM(+1), the cooling SST trend is stronger in the Niño-3 region, contributed mostly by

atmospheric forcing; while oceanic horizontal advection is dominant for SST change during all of the ensuing season and is responsible for the SST cooling trend after MAM(+1) in the Niño-4 region.

The contributions of different components of net heat flux are further investigated. SW, LW, and LHF are closely related with the preceding IOD forcing, especially before the ensuing summer [JJA(+1)]. Among them, from SON(0) to MAM(+1), the SW anomalies contribute to the SST cooling over the

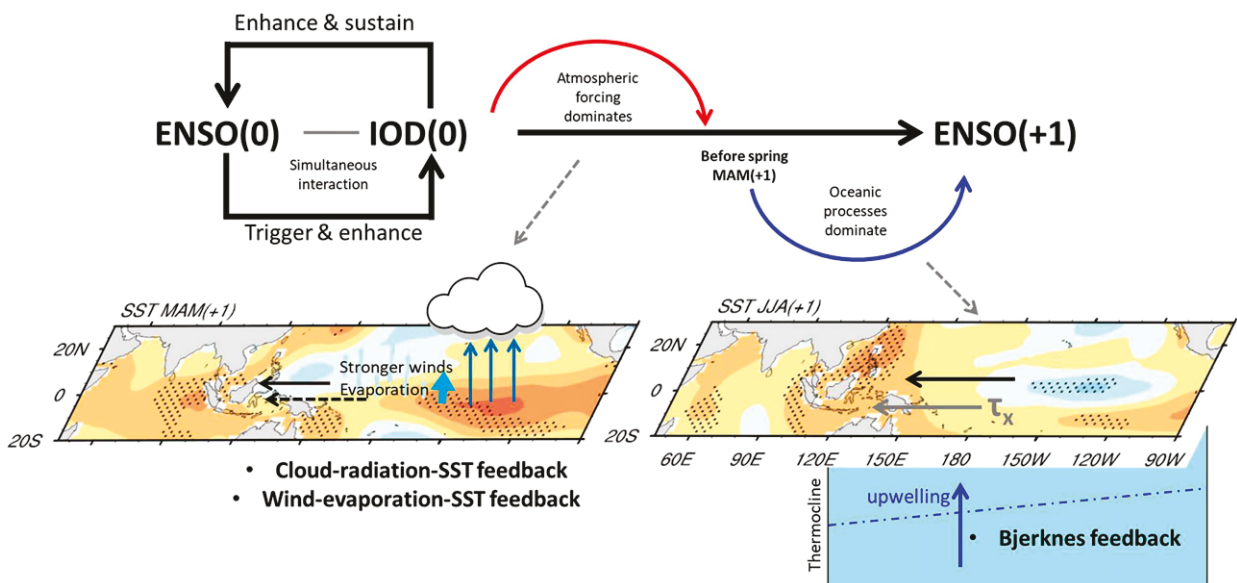


FIG. 16. Schematic illustration of the interaction between the IOD and ENSO.

central and eastern Pacific, which is likely associated with the increase in cloudiness and precipitation caused by the warm SST forcing over the equatorial Pacific. As a result, the cloud–radiation effect can be identified. LHF is important from DJF(+1) to JJA(+1), especially in the equatorial central Pacific.

As indicated by the variations in LHF evolution, from DJF(+1) the wind–evaporation–SST feedback should be important for the Pacific. After autumn, zonal alternation from westerlies to easterlies gradually occurs from the western to the eastern Pacific, contributing to the escalation of wind speed, which consequently can strengthen evaporation and cool down the SST.

The mechanism by which the IOD favors the development of the subsequent ENSO after the ensuing spring can be explained by the local Bjerknes feedback. The SSH response, a proxy of the thermocline, displays an eastward-propagating negative response to the preceding IOD with a maximum correlation in the central Pacific after the ensuing spring. Such thermocline shoaling variations are the consequence of oceanic divergence and easterly anomalies over the central Pacific, which can in turn cause anomalous cold water upwelling, cooling the SST. The SST cooling and the thermocline uplift over the equatorial Pacific also suggest that WWV is decreasing over the equatorial Pacific, which is basically a discharge process and is also able to initiate a La Niña case according to the “recharge–discharge” mechanism for ENSO (Jin 1997a,b).

The simultaneous relationship between the IOD and ENSO has long been investigated: previous work has revealed that ENSO(0) is an important trigger mechanism for IOD(0) oscillation and can also strengthen the intensity of IOD(0); on the other hand, IOD(0) can also amplify the intensity of ENSO(0) and is indicated to favor the demise of ENSO(0) (e.g., Luo et al. 2010). In terms of the lead–lag relationship between IOD(0) and ENSO(+1), studies so far are quite limited. However, this study confirms that the IOD can influence the evolution of the subsequent ENSO(+1) and can be an important component in sustaining the tropical tropospheric biennial oscillation (TBO, e.g., Meehl 1997). The interaction between these major modes is schematically illustrated in Fig. 16. Considering these new findings, some previous conclusions that suggest that Indian Ocean coupling is important to ENSO predictions may be essentially related to the IOD. Further study is therefore needed to further clarify the relative contributions of the IOD and IOB to SST changes over the equatorial Pacific in the next year. These findings may also lead to a new method of combining the IOD with the subsequent ENSO to improve the long-term predictability of the ocean–atmosphere system.

Acknowledgments. This work was supported by National Natural Science Foundation of China Grants 42005010 and 41675062 and the Hong Kong RGC General Research Fund 11306417.

REFERENCES

- Alexander, M. A., I. Bladé, M. Newman, J. R. Lanzante, N. Lau, and J. D. Scott, 2002: The atmospheric bridge: The influence of ENSO teleconnections on air–sea interaction over the global oceans. *J. Climate*, **15**, 2205–2231, [https://doi.org/10.1175/1520-0442\(2002\)015<2205:TABTIO>2.0.CO;2](https://doi.org/10.1175/1520-0442(2002)015<2205:TABTIO>2.0.CO;2).
- Annamalai, H., R. Murtugudde, J. Potemra, S. P. Xie, P. Liu, and B. Wang, 2003: Coupled dynamics over the Indian Ocean: Spring initiation of the zonal mode. *Deep-Sea Res. II*, **50**, 2305–2330, [https://doi.org/10.1016/S0967-0645\(03\)00058-4](https://doi.org/10.1016/S0967-0645(03)00058-4).
- , S. P. Xie, J. P. McCreary, and R. Murtugudde, 2005: Impact of Indian Ocean sea surface temperature on developing El Niño. *J. Climate*, **18**, 302–319, <https://doi.org/10.1175/JCLI-3268.1>.
- Ashok, K., Z. Guan, N. H. Saji, and T. Yamagata, 2004: Individual and combined influences of ENSO and the Indian Ocean dipole on the Indian summer monsoon. *J. Climate*, **17**, 3141–3155, [https://doi.org/10.1175/1520-0442\(2004\)017<3141:IACIOE>2.0.CO;2](https://doi.org/10.1175/1520-0442(2004)017<3141:IACIOE>2.0.CO;2).
- Behera, S. K., J. J. Luo, S. Masson, S. A. Rao, H. Sakuma, and T. Yamagata, 2006: A CGCM study on the interaction between IOD and ENSO. *J. Climate*, **19**, 1688–1705, <https://doi.org/10.1175/JCLI3797.1>.
- Berry, D. I., and E. C. Kent, 2009: A new air–sea interaction gridded dataset from ICOADS with uncertainty estimates. *Bull. Amer. Meteor. Soc.*, **90**, 645–656, <https://doi.org/10.1175/2008BAMS2639.1>.
- , and —, 2011: Air–sea fluxes from ICOADS: The construction of a new gridded dataset with uncertainty estimates. *Int. J. Climatol.*, **31**, 987–1001, <https://doi.org/10.1002/joc.2059>.
- Cai, W., P. van Rensch, T. Cowan, and H. H. Hendon, 2011: Teleconnection pathways of ENSO and the IOD and the mechanisms for impacts on Australian rainfall. *J. Climate*, **24**, 3910–3923, <https://doi.org/10.1175/2011JCLI4129.1>.
- Carton, J. A., and B. S. Giese, 2008: A reanalysis of ocean climate using Simple Ocean Data Assimilation (SODA). *Mon. Wea. Rev.*, **136**, 2999–3017, <https://doi.org/10.1175/2007MWR1978.1>.
- Chen, J., X. Wang, W. Zhou, and Z. Wen, 2018a: Interdecadal change in the summer SST–precipitation relationship around the late 1990s over the South China Sea. *Climate Dyn.*, **51**, 2229–2246, <https://doi.org/10.1007/s00382-017-4009-y>.
- , —, —, C. Wang, Q. Xie, G. Li, and S. Chen, 2018b: Unusual rainfall in southern China in decaying August during extreme El Niño 2015/16: Role of the western Indian Ocean and north tropical Atlantic SST. *J. Climate*, **31**, 7019–7034, <https://doi.org/10.1175/JCLI-D-17-0827.1>.
- Chen, M., T. Li, X. Shen, and B. Wu, 2016: Relative roles of dynamic and thermodynamic processes in causing evolution asymmetry between El Niño and La Niña. *J. Climate*, **29**, 2201–2220, <https://doi.org/10.1175/JCLI-D-15-0547.1>.
- Chen, W., J. Feng, and R. Wu, 2013: Roles of ENSO and PDO in the link of the East Asian winter monsoon to the following summer monsoon. *J. Climate*, **26**, 622–635, <https://doi.org/10.1175/JCLI-D-12-00021.1>.
- Dayan, H., J. Vialard, T. Izumo, and M. Lengaigne, 2014: Does sea surface temperature outside the tropical Pacific contribute to enhanced ENSO predictability? *Climate Dyn.*, **43**, 1311–1325, <https://doi.org/10.1007/s00382-013-1946-y>.
- Dee, D. P., and Coauthors, 2011: The ERA-Interim reanalysis: Configuration and performance of the data assimilation system. *Quart. J. Roy. Meteor. Soc.*, **137**, 553–597, <https://doi.org/10.1002/qj.828>.
- Dong, L., and M. J. McPhaden, 2017: Why has the relationship between Indian and Pacific Ocean decadal variability changed in recent decades? *J. Climate*, **30**, 1971–1983, <https://doi.org/10.1175/JCLI-D-16-0313.1>.
- Fischer, A. S., P. Terray, E. Guilyardi, S. Gualdi, and P. Delecluse, 2005: Two independent triggers for the Indian Ocean dipole/zonal mode in a coupled GCM. *J. Climate*, **18**, 3428–3449, <https://doi.org/10.1175/JCLI3478.1>.

- Gu, W., C. Li, X. Wang, W. Zhou, and W. Li, 2009: Linkage between mei-yu precipitation and North Atlantic SST on the decadal timescale. *Adv. Atmos. Sci.*, **26**, 101–108, <https://doi.org/10.1007/s00376-009-0101-5>.
- Gualdi, S., E. Guilyardi, A. Navarra, S. Masina, and P. Delecluse, 2003: The interannual variability in the tropical Indian Ocean as simulated by a CGCM. *Climate Dyn.*, **20**, 567–582, <https://doi.org/10.1007/s00382-002-0295-z>.
- Ham, Y.-G., J.-S. Kug, and J.-Y. Park, 2013: Two distinct roles of Atlantic SSTs in ENSO variability: North tropical Atlantic SST and Atlantic Niño. *Geophys. Res. Lett.*, **40**, 4012–4017, <https://doi.org/10.1002/grl.50729>.
- He, Z., and R. Wu, 2013: Coupled seasonal variability in the South China Sea. *J. Oceanogr.*, **69**, 57–69, <https://doi.org/10.1007/s10872-012-0157-1>.
- Huang, B., and Coauthors, 2017: Extended reconstructed sea surface temperature, version 5 (ERSSTv5): Upgrades, validations, and intercomparisons. *J. Climate*, **30**, 8179–8205, <https://doi.org/10.1175/JCLI-D-16-0836.1>.
- Izumo, T., and Coauthors, 2010: Influence of the state of the Indian Ocean dipole on the following year's El Niño. *Nat. Geosci.*, **3**, 168–172, <https://doi.org/10.1038/ngeo760>.
- , M. Lengaigne, J. Vialard, J. J. Luo, T. Yamagata, and G. Madec, 2014: Influence of Indian Ocean dipole and Pacific recharge on following year's El Niño: Interdecadal robustness. *Climate Dyn.*, **42**, 291–310, <https://doi.org/10.1007/s00382-012-1628-1>.
- , J. Vialard, H. Dayan, M. Lengaigne, and I. Suresh, 2016: A simple estimation of equatorial Pacific response from wind-stress to untangle Indian Ocean dipole and basin influences on El Niño. *Climate Dyn.*, **46**, 2247–2268, <https://doi.org/10.1007/s00382-015-2700-4>.
- Jiang, X.-A., and T. Li, 2005: Reinitiation of the boreal summer intraseasonal oscillation in the tropical Indian Ocean. *J. Climate*, **18**, 3777–3795, <https://doi.org/10.1175/JCLI3516.1>.
- Jin, F. F., 1997a: An equatorial ocean recharge paradigm for ENSO. Part I: Conceptual model. *J. Atmos. Sci.*, **54**, 811–829, [https://doi.org/10.1175/1520-0469\(1997\)054<0811:AEORPF>2.0.CO;2](https://doi.org/10.1175/1520-0469(1997)054<0811:AEORPF>2.0.CO;2).
- , 1997b: An equatorial ocean recharge paradigm for ENSO. Part II: A stripped-down coupled model. *J. Atmos. Sci.*, **54**, 830–847, [https://doi.org/10.1175/1520-0469\(1997\)054<0830:AEORPF>2.0.CO;2](https://doi.org/10.1175/1520-0469(1997)054<0830:AEORPF>2.0.CO;2).
- Kim, W., W. Cai, and J.-S. Kug, 2015: Migration of atmospheric convection coupled with ocean currents pushes El Niño to extremes. *Geophys. Res. Lett.*, **42**, 3583–3590, <https://doi.org/10.1002/2015GL063886>.
- Kripalani, R. H., J. H. Oh, and H. S. Chaudhari, 2010: Delayed influence of the Indian Ocean dipole mode on the East Asia–west Pacific monsoon: Possible mechanism. *Int. J. Climatol.*, **30**, 197–209, <https://doi.org/10.1002/joc.1890>.
- Kug, J. S., and I. S. Kang, 2006: Interactive feedback between ENSO and the Indian Ocean. *J. Climate*, **19**, 1784–1801, <https://doi.org/10.1175/JCLI3660.1>.
- , T. Li, S. Il An, I. S. Kang, J. J. Luo, S. Masson, and T. Yamagata, 2006: Role of the ENSO–Indian Ocean coupling on ENSO variability in a coupled GCM. *Geophys. Res. Lett.*, **33**, L09710, <https://doi.org/10.1029/2005GL024916>.
- Lee, H.-T., A. Gruber, R. G. Ellingson, I. Laszlo, H.-T. Lee, A. Gruber, R. G. Ellingson, and I. Laszlo, 2007: Development of the HIRS outgoing longwave radiation climate dataset. *J. Atmos. Oceanic Technol.*, **24**, 2029–2047, <https://doi.org/10.1175/2007JTECHA989.1>.
- Leung, M. Y. T., H. H. N. Cheung, and W. Zhou, 2017: Meridional displacement of the East Asian trough and its response to the ENSO forcing. *Climate Dyn.*, **48**, 335–352, <https://doi.org/10.1007/s00382-016-3077-8>.
- , W. Zhou, D. Wang, P. W. Chan, S. M. Lee, and H. W. Tong, 2020: Remote tropical western Indian Ocean forcing on changes in June precipitation in South China and the Indochina Peninsula. *J. Climate*, **33**, 7553–7566, <https://doi.org/10.1175/JCLI-D-19-0626.1>.
- Li, R. C. Y., W. Zhou, and T. Li, 2014: Influences of the Pacific–Japan teleconnection pattern on synoptic-scale variability in the western North Pacific. *J. Climate*, **27**, 140–154, <https://doi.org/10.1175/JCLI-D-13-00183.1>.
- Li, T., 2006: Origin of the summertime synoptic-scale wave train in the western North Pacific. *J. Atmos. Sci.*, **63**, 1093–1102, <https://doi.org/10.1175/JAS3676.1>.
- , B. Wang, B. Wu, T. Zhou, C. P. Chang, and R. Zhang, 2017: Theories on formation of an anomalous anticyclone in western North Pacific during El Niño: A review. *J. Meteor. Res.*, **31**, 987–1006, <https://doi.org/10.1007/s13351-017-7147-6>.
- Li, X., and C. Li, 2017: The tropical Pacific–Indian Ocean associated mode simulated by LICOM2.0. *Adv. Atmos. Sci.*, **34**, 1426–1436, <https://doi.org/10.1007/s00376-017-6176-5>.
- Luo, J.-J., S. Behera, Y. Masumoto, H. Sakuma, and T. Yamagata, 2008: Successful prediction of the consecutive IOD in 2006 and 2007. *Geophys. Res. Lett.*, **35**, L14S02, <https://doi.org/10.1029/2007GL032793>.
- , R. Zhang, S. K. Behera, Y. Masumoto, F. F. Jin, R. Lukas, and T. Yamagata, 2010: Interaction between El Niño and extreme Indian Ocean dipole. *J. Climate*, **23**, 726–742, <https://doi.org/10.1175/2009JCLI3104.1>.
- McPhaden, M. J., S. E. Zebiak, and M. H. Glantz, 2006: ENSO as an integrating concept in earth science. *Science*, **314**, 1740–1745, <https://doi.org/10.1126/science.1132588>.
- Meehl, G. A., 1997: The South Asian monsoon and the tropospheric biennial oscillation. *J. Climate*, **10**, 1921–1943, [https://doi.org/10.1175/1520-0442\(1997\)010<1921:TSAMAT>2.0.CO;2](https://doi.org/10.1175/1520-0442(1997)010<1921:TSAMAT>2.0.CO;2).
- Ohba, M., and H. Ueda, 2007: An impact of SST anomalies in the Indian Ocean in acceleration of the El Niño to La Niña transition. *J. Meteor. Soc. Japan*, **85**, 335–348, <https://doi.org/10.2151/jmsj.85.335>.
- , and M. Watanabe, 2012: Role of the Indo-Pacific interbasin coupling in predicting asymmetric ENSO transition and duration. *J. Climate*, **25**, 3321–3335, <https://doi.org/10.1175/JCLI-D-11-00409.1>.
- Peng, Q., S. P. Xie, D. Wang, Y. Kamae, H. Zhang, S. Hu, X. T. Zheng, and W. Wang, 2020: Eastern Pacific wind effect on the evolution of El Niño: Implications for ENSO diversity. *J. Climate*, **33**, 3197–3212, <https://doi.org/10.1175/JCLI-D-19-0435.1>.
- Rasmusson, E. M., and T. H. Carpenter, 1982: Variations in tropical sea surface temperature and surface wind fields associated with the Southern Oscillation/El Niño (Pacific). *Mon. Wea. Rev.*, **110**, 354–384, [https://doi.org/10.1175/1520-0493\(1982\)110<0354:VITSSST>2.0.CO;2](https://doi.org/10.1175/1520-0493(1982)110<0354:VITSSST>2.0.CO;2).
- Saji, N. H., and T. Yamagata, 2003: Possible impacts of Indian Ocean dipole mode events on global climate. *Climate Res.*, **25**, 151–169, <https://doi.org/10.3354/cr025151>.
- , B. N. Goswami, P. N. Vinayachandran, and T. Yamagata, 1999: A dipole mode in the tropical Indian Ocean. *Nature*, **401**, 360–363, <https://doi.org/10.1038/43854>.
- Santoso, A., M. J. McPhaden, and W. Cai, 2017: The defining characteristics of ENSO extremes and the strong 2015/2016 El Niño. *Rev. Geophys.*, **55**, 1079–1129, <https://doi.org/10.1002/2017RG000560>.

- Ueda, H., and J. Matsumoto, 2000: A possible triggering process of east–west asymmetric anomalies over the Indian Ocean in relation to 1997/98 El Niño. *J. Meteor. Soc. Japan*, **78**, 803–818, https://doi.org/10.2151/jmsj1965.78.6_803.
- Wang, B., R. Wu, and X. Fu, 2000: Pacific–East Asian teleconnection: How does ENSO affect East Asian climate? *J. Climate*, **13**, 1517–1536, [https://doi.org/10.1175/1520-0442\(2000\)013<1517:PEATHD>2.0.CO;2](https://doi.org/10.1175/1520-0442(2000)013<1517:PEATHD>2.0.CO;2).
- , —, and T. Li, 2003: Atmosphere–warm ocean interaction and its impacts on Asian–Australian monsoon variation. *J. Climate*, **16**, 1195–1211, [https://doi.org/10.1175/1520-0442\(2003\)16<1195:AIOIAH>2.0.CO;2](https://doi.org/10.1175/1520-0442(2003)16<1195:AIOIAH>2.0.CO;2).
- Wang, D., Y. Qin, X. Xiao, Z. Zhang, and X. Wu, 2012: El Niño and El Niño Modoki variability based on a new ocean reanalysis. *Ocean Dyn.*, **62**, 1311–1322, <https://doi.org/10.1007/s10236-012-0566-0>.
- Wang, W., W. Zhou, D. Chen, W. Wang, W. Zhou, and D. Chen, 2014: Summer high temperature extremes in southeast China: Bonding with the El Niño–Southern Oscillation and East Asian summer monsoon coupled system. *J. Climate*, **27**, 4122–4138, <https://doi.org/10.1175/JCLI-D-13-00545.1>.
- Wang, X., C. Li, and W. Zhou, 2006: Interdecadal variation of the relationship between Indian rainfall and SSTA modes in the Indian Ocean. *Int. J. Climatol.*, **26**, 595–606, <https://doi.org/10.1002/joc.1283>.
- , D. Wang, and W. Zhou, 2009: Decadal variability of twentieth-century El Niño and La Niña occurrence from observations and IPCC AR4 coupled models. *Geophys. Res. Lett.*, **36**, L11701, <https://doi.org/10.1029/2009GL037929>.
- , W. Zhou, C. Li, and D. Wang, 2014: Comparison of the impact of two types of El Niño on tropical cyclone genesis over the South China Sea. *Int. J. Climatol.*, **34**, 2651–2660, <https://doi.org/10.1002/joc.3865>.
- Watanabe, M., and F. Jin, 2002: Role of Indian Ocean warming in the development of Philippine Sea anticyclone during ENSO. *Geophys. Res. Lett.*, **29**, 1478, <https://doi.org/10.1029/2001GL014318>.
- Webster, P. J., and S. Yang, 1992: Monsoon and ENSO: Selectively interactive systems. *Quart. J. Roy. Meteor. Soc.*, **118**, 877–926, <https://doi.org/10.1002/qj.49711850705>.
- , A. Moore, J. P. Loschnigg, and R. R. Leben, 1999: Coupled ocean–atmosphere dynamics in the Indian Ocean during 1997–98. *Nature*, **401**, 356–360, <https://doi.org/10.1038/43848>.
- Wu, B., T. Zhou, and T. Li, 2009a: Seasonally evolving dominant interannual variability modes of East Asian climate. *J. Climate*, **22**, 2992–3005, <https://doi.org/10.1175/2008JCLI2710.1>.
- , —, and —, 2009b: Contrast of rainfall–SST relationships in the western North Pacific between the ENSO-developing and ENSO-decaying summers. *J. Climate*, **22**, 4398–4405, <https://doi.org/10.1175/2009JCLI2648.1>.
- Wu, R., and B. P. Kirtman, 2004: Understanding the impacts of the Indian Ocean on ENSO variability in a coupled GCM. *J. Climate*, **17**, 4019–4031, [https://doi.org/10.1175/1520-0442\(2004\)017<4019:UTIOTI>2.0.CO;2](https://doi.org/10.1175/1520-0442(2004)017<4019:UTIOTI>2.0.CO;2).
- Xie, S.-P., K. M. Hu, J. Hafner, H. Tokinaga, Y. Du, G. Huang, and T. Sampe, 2009: Indian Ocean capacitor effect on Indo-western Pacific climate during the summer following El Niño. *J. Climate*, **22**, 730–747, <https://doi.org/10.1175/2008JCLI2544.1>.
- Yamanaka, G., T. Yasuda, Y. Fujii, and S. Matsumoto, 2009: Rapid termination of the 2006 El Niño and its relation to the Indian Ocean. *Geophys. Res. Lett.*, **36**, L07702, <https://doi.org/10.1029/2009GL037298>.
- Yu, J.-Y., 2005: Enhancement of ENSO’s persistence barrier by biennial variability in a coupled atmosphere–ocean general circulation model. *Geophys. Res. Lett.*, **32**, L13707, <https://doi.org/10.1029/2005GL023406>.
- , C. R. Mechoso, J. C. McWilliams, and A. Arakawa, 2002: Impacts of the Indian Ocean on the ENSO cycle. *Geophys. Res. Lett.*, **29**, 1204, <https://doi.org/10.1029/2001GL014098>.
- Yuan, Y., J. C. L. Chan, W. Zhou, and C. Li, 2008a: Decadal and interannual variability of the Indian Ocean dipole. *Adv. Atmos. Sci.*, **25**, 856–866, <https://doi.org/10.1007/s00376-008-0856-0>.
- , H. Yang, W. Zhou, and C. Li, 2008b: Influences of the Indian Ocean dipole on the Asian summer monsoon in the following year. *Int. J. Climatol.*, **28**, 1849–1859, <https://doi.org/10.1002/joc.1678>.
- , W. Zhou, H. Yang, and C. Li, 2008c: Warming in the northwestern Indian Ocean associated with the El Niño event. *Adv. Atmos. Sci.*, **25**, 246–252, <https://doi.org/10.1007/s00376-008-0246-7>.
- Zhang, W., Y. Wang, F.-F. Jin, M. F. Stuecker, and A. G. Turner, 2015: Impact of different El Niño types on the El Niño/IOD relationship. *Geophys. Res. Lett.*, **42**, 8570–8576, <https://doi.org/10.1002/2015GL065703>.
- Zhang, Y., W. Zhou, E. C. H. Chow, and M. Y. T. Leung, 2019a: Delayed impacts of the IOD: Cross-seasonal relationships between the IOD, Tibetan Plateau snow, and summer precipitation over the Yangtze–Huaihe River region. *Climate Dyn.*, **53**, 4077–4093, <https://doi.org/10.1007/s00382-019-04774-5>.
- , —, and M. Y. T. Leung, 2019b: Phase relationship between summer and winter monsoons over the South China Sea: Indian Ocean and ENSO forcing. *Climate Dyn.*, **52**, 5229–5248, <https://doi.org/10.1007/s00382-018-4440-8>.